Real-Time Measurements of Cell Proliferation Using a Lab-on-CMOS Capacitance Sensor Array

Bathiya Prashan Senevirathna, *Student Member, IEEE*, Sheung Lu, *Student Member, IEEE*, Marc P. Dandin, *Senior Member, IEEE*, John Basile, Elisabeth Smela, *Member, IEEE*, and Pamela A. Abshire, *Fellow, IEEE*

***Abstract*—We describe a capacitance sensor array that has been incorporated into a lab-on-CMOS system for applications in monitoring cell viability. This paper presents analytical models, calibration results, and measured experimental results of the biosensor. The sensor has been characterized and exhibits a sensitivity of 590 kHz/fF. We report results from benchtop tests and *in vitro* experiments demonstrating on-chip tracking of cell adhesion as well as monitoring of cell viability. Human ovarian cancer cells were cultured on chip, and measured capacitance responses were validated by comparison with images from photomicrographs of the chip surface. Analysis was performed to quantify cell proliferation and adhesion, and responses to live cells were estimated to be 100 aF/cell.**

***Index Terms*—Capacitance measurement, cell culture, CMOS integrated circuits, dielectric measurements, lab on a chip, mixed analog-digital integrated circuits.**

I. Introduction

MICROELECTRONIC biosensors have the potential to provide low-cost, flexible, and portable devices for applications in fields such as biology, environmental science, and medicine. A ubiquitous experimental challenge is to monitor the proliferation of cells over time to determine their response to stimuli or environmental conditions. Monitoring cell growth and migration is an important tool for optimizing cell culture conditions, testing drugs, and screening materials for biocompatibility and toxicity. Conventional approaches involve the use of dyes and markers that can potentially introduce side-effects into the cell culture and often function as end-point assays, eliminating the opportunity to track fast changes and to determine temporal correlation between measurements. Therefore it is important to develop new techniques to perform these measurements. Lab-on-chip devices have shown great promise in changing the way that biological samples are analyzed. They allow for smaller sample volumes, reduced cost, faster reaction kinetics, and higher throughput than conventional approaches. Another important advantage of lab-on-chip systems is their potential for automated and unsupervised data collection. In most instances, however, lab-on-chip devices comprise a passive sensing layer that requires external instrumentation for readout and signal processing [1], [2]. Recently, CMOS technology has become an important platform for lab-on-chip systems since it facilitates the incorporation of sensing and actuation in intimate contact with readout and electronics, producing systems with smaller size, higher sensing density, and higher sensing fidelity. CMOS technology offers the advantages of having low static power requirements and good noise immunity, as well as being widely available and facilitating integration with commercial electronics.

Several lab-on-CMOS systems have been previously developed for the purpose of monitoring cell proliferation (discussed in Section II). These sensors have shown efficacy in detecting the growth of cells; however these designs generally still require significant external hardware for readout and so do not readily lend themselves for portable applications. In this paper we report the use of a capacitance sensor array on the surface of an integrated circuit chip to measure an analogue of cell health. The reported biosensors provide the ability to automate and expand measurements beyond the capabilities of traditional laboratory equipment. The sensors are amenable to portable applications and provide a quantitative digital readout that reflects the graded dynamical behavior of cell-substrate coupling.

This paper describes the implementation of a ring oscillator-based capacitance sensor [3], including implementation of the readout, experimental results, analytical models, calibration of the sensor, and biological validation *in vitro*. The sensor exhibits a sensitivity of 590 kHz/fF, resolution of 14.4 aF, and an input sensing range of 12 fF. In addition to dry bench-top testing, the chip was packaged for operation in a cell culture environment

Manuscript received October 27, 2017; revised January 28, 2018 and March 13, 2018; accepted March 14, 2018. Date of publication May 15, 2018; date of current version June 5, 2018. This work was supported in part by the UMD-UMB Research and Innovation Seed Grant and in part by the Academy of Finland (The ClintoxNP project #268944). This paper was recommended by Associate Editor M. Kalofonou. *(Corresponding author: Bathiya Prashan Senevirathna.)*

B. P. Senevirathna, S. Lu, and P. A. Abshire are with the Department of Electrical and Computer Engineering and the Institute for Systems Research, University of Maryland, College Park, MD 20742 USA (e-mail: bsenevir@umd.edu; sheunglu@umd.edu; pabshire@umd.edu).

M. P. Dandin was with the Fischell Department of Bioengineering and the Institute for Systems Research, University of Maryland, College Park, MD 20742 USA. He is now with the Kiskeya Microsystems, Rockville, MD 20851 USA (e-mail: info@kmicro.systems).

J. Basile is with the Department of Oncology and Diagnostic Sciences, University of Maryland School of Dentistry, Baltimore, MD 21201 USA (e-mail: jbasile@umaryland.edu).

E. Smela is with the Department of Mechanical Engineering and the Institute for Systems Research, University of Maryland, College Park, MD 20742 USA (e-mail: smela@umd.edu).

This paper has supplementary downloadable material available at http://ieeexplore.ieee.org, provided by the author.

Color versions of one or more of the figures in this paper are available online at http://ieeexplore.ieee.org.

Digital Object Identifier 10.1109/TBCAS.2018.2821060

and tested with organic fluids with varying dielectric constants and with cultures of two different cancer cell lines. Different aspects of the sensor system were reported in three earlier conference papers. The sensor design was initially reported in [4], its integration into a system with I^2C readout was reported in [5], and initial benchtop characterization results were reported in [3]. This paper extends the prior work by presenting the results from *in vitro* experiments with cultured cells and validating those results through visual observation.

II. Cell Adhesion and Viability

Cell adhesion is an important initial step in cell growth, signaling, and regulating cell behavior [6], [7]. Many commonly studied cells are anchorage-dependent, meaning that they are unable to proliferate when cultured in suspension and require a substrate on which to grow. Healthy anchorage-dependent cells have stronger adhesion with an underlying substrate than unhealthy or dead cells. Therefore the study of cell adhesion can be used as an analogue for studying cell viability. This in turn allows for greater insight into how cells grow and proliferate, and their susceptibility to chemical agents. Studies of cell adhesion have been performed in various applications such as wound healing and cancer research [8]–[10].

A. Characterizing Cell Adhesion

Several non-electronic approaches to characterizing cell adhesion involve the use of specialized equipment. In traction force microscopy, cells are cultured on a functionalized polyacrylamide gel in which fluorescent beads have been embedded. When cells adhere, they generate traction forces that can be quantified by monitoring the locations of the fluorescent beads [11]. Cells have also been exposed to shear fluid flow in microfluidic channels [12]. The adhesion strength is related to the number of cells remaining after exposure to the disruptive fluid forces. Force has also been applied to detach cells directly using a micropipette; this technique requires specialized equipment for precise probe manipulation. The micropipette applies suction force to the top of a cell, and the aspiration pressure required to pull the cell off the substrate is a measure of its adhesion strength [13]. Optical techniques include approaches such as dye exclusion and fluorescence spectroscopy and typically require microscopes and optical filters for measurement. Methods that require the addition of a dye or fluorescent agent can compromise viability and lead to cell death [14]. Additionally these approaches require sampling of the analyte which might not be feasible for small culture volumes. Therefore a label-free detection method would be beneficial. Furthermore, many traditional characterization methods are end-point assays which provide a measure of adhesion only at the end of an experimental procedure. Many parallel experiments are required to obtain a temporal sequence of discrete sample points, with temporal accuracy limited by the variability across samples and the sampling technique. Much richer information about the dynamics of cell growth would be available from a real-time measurement methodology.

A number of physical transduction mechanisms have been introduced for monitoring biological cells. Impedance spectroscopy, quartz crystal microbalances, and surface acoustic waves [15]–[17], commonly used for characterization of material properties, have been used to study cells; however they generally require large external equipment for readout. Ion-sensitive FETs have also been used to detect bacterial activity [18], however they are generally used to measure analogues of cell activity (such as pH changes), rather than viability directly. Amperometry has also been used in cell detection [19], however post-fabrication of electrodes on CMOS chips are required. CMOS-based capacitance sensors have been developed for a number of cell monitoring applications. These chips implement arrays of sensing electrodes that detect capacitive changes as cells adhere to and grow across the surface of the chip. The electrodes are insulated from the cell culture environment and so limit undesirable electrochemistry that may otherwise occur.

B. Capacitive Sensing Approach

The measurement of capacitive loading on the substrate as cells grow and proliferate can be performed using several different transduction methods. These include charge-based capacitance measurement (CBCM), charge sharing (CS), electric cell-substrate impedance, and capacitance-to-frequency (CTF) methods [20]–[27].

Prakash *et al*. implemented CS and differential CBCM designs for characterizing cell adhesion [20], [21], [28] and presented *in vitro* measurements of muscle cells and cancer cell lines. Ghafar-Zadeh *et al*. used a CBCM structure to monitor the growth of bacteria in medium [25]. Nabovati *et al*. used a differential CBCM structure for cell monitoring [29], and more recently extended the design to an 8×8 array [30]. This system included a $\Sigma\Delta$ ADC to convert the output voltage to a serial stream of bits that was read off-chip using an FPGA. CBCM sensors have high sensing resolution and relatively small chip area requirements but they are sensitive to parasitic mismatches. The sensing paradigm relies on symmetrical circuit topologies, so mismatches cause an unwanted offset at the output voltage, which can limit dynamic range significantly [30], [31]. One way to counter this is to implement floating-gate trimming circuits to alter the charge on the CBCM current mirrors after fabrication [31]. Alternatively, a bank of current mirrors can be used to tune the CBCM charging current through auto-calibration [22], [30].

These systems require a complex readout system and initial setup protocols. Capacitance-to-frequency based transduction systems offer an alternative approach that is inherently tolerant to large offset capacitances and parasitic mismatch. This is because the output signal is an oscillation frequency which can vary by orders of magnitude in response to large changes in capacitance. In contrast, the voltage output of CBCM techniques is limited by the rail voltages. Additionally, CTF schemes can resolve minute changes in capacitance by integrating the output over a longer period of time. This means that both slow signals (large capacitances) and fast signals (small capacitances) can be read using a single chip. Furthermore, frequency based systems are inherently suited for digitization because the output signal

can be treated as a digital "clock". This obviates the need for a traditional ADC, leading to a smaller footprint on-chip.

In this work we present a CTF-based sensor for cell viability monitoring and quantification that offers distinct advantages over prior work. The system is simple, requiring only a low cost commercially available microcontroller to operate. The entire system including the microcontroller consumes 300 mW of power with the IC chip alone consuming 8 mW, enabling the design's use in portable applications. The system allows for multiple chips to be recording in parallel without the need for additional hardware, allowing for high-throughput assays. It can operate unsupervised with higher temporal resolution than traditional assays. We also present results and analysis from *in vitro* experiments with living biological cells that affirm the system's use for biological assays.

III. Cell Capacitance Sensing

This paper presents the design of a custom capacitance sensor lab-on-CMOS chip. The sensor implements a 4 × 4 array of interdigitated electrodes with digitization on chip and automatic data readout using a serial bus. The chip was designed to allow for simple implementation and ease of experimentation. It utilizes a microcontroller for data readout and storage.

A. Sensor Design

A schematic of an individual capacitance sensor is shown in Fig. 1(a) [3], [5]. The sensor utilizes a capacitance-to-frequency transduction mechanism. The sensor consists of a three-stage ring oscillator with two of its nodes connected to interdigitated electrodes which are fabricated in the top-most metal layer of the CMOS technology and act as the sensing plates. The capacitance sensed on these 30 × 30 μm^2 interdigitated electrodes (shown in Fig. 1(b)) load the oscillator, causing changes in its charging and discharging rates, leading to a change in the oscillation frequency [5]. Parasitic load capacitances at each inverter stage in the oscillator $(C_{L1} - C_{L3})$ introduce finite switching delays $(\tau_1 - \tau_3)$, and these contribute to the total delay period, which leads to the oscillation frequency of the sensor:

$$f = \frac{I_B}{V_{TH}\left(C_{L1} + C_{L2} + C_{L3}\right)} \tag{1}$$

where V_{TH} is the MOSFET threshold voltage and I_B is the bias current. The interdigitated electrode contributes an input capacitance, C_{IN}, to one stage of the ring oscillator. For each switching transition, this capacitance is discharged and charged in opposing directions, increasing the effective capacitance across the inverter. The delay period of this input stage can be written as [32]:

$$\tau_2 = \frac{V_{DD}}{I_B}\left(C_{L2} + 3C_{IN}\right) \tag{2}$$

This produces a hyperbolic change in frequency as the input capacitance changes. However, under the expected operating conditions and for small variations in sensed capacitance, the capacitance-frequency relationship can be approximated as linear. This was confirmed through SPICE simulations by sweeping input capacitance over a 2 fF range, resulting in output frequencies that show a linear trend (R^2 value of 0.99) [5]. Benchtop experiments additionally support this observation as discussed in Section IV-A (Fig. 2).

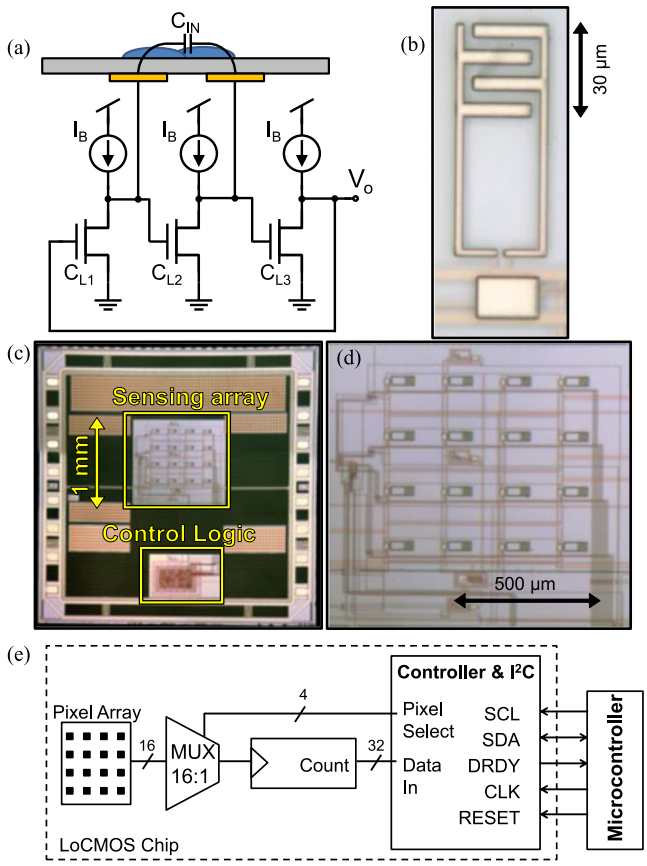

Fig. 1. (a) Circuit diagram of capacitance sensor pixel. Photomicrograph of (b) sensing electrodes (30 × 30 μm^2), (c) fabricated die (3 × 3 mm^2), and (d) sensing array. (e) System block diagram.

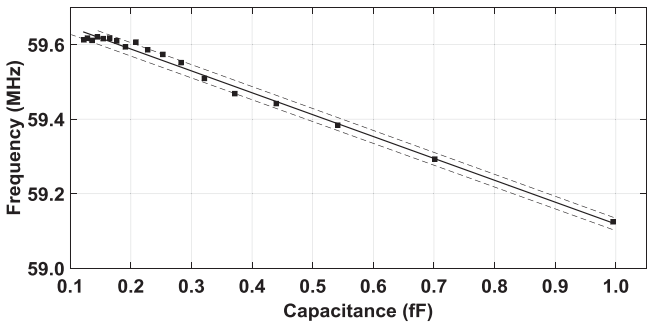

Fig. 2. Sensor characterization curve generated by mapping electrode probe distance to modeled capacitance value.

B. System Architecture

Fig. 1(e) shows a block diagram of the system. The capacitance sensor chip was designed with an array of 4 × 4 sensor pixels. Each pixel's output passes through a digital buffer into a multiplexer, which then connects to a 32-bit counter. The

counter integrates the oscillating signal for a specified duration (see Section III-C). Once the integration time is reached, the final count value is sent off-chip via an I^2C interface implemented on chip. The NMOS transistors making up the oscillators are sized with a width-to-length ratio of 2.8/0.7 μm. The transistor sizing was chosen to produce a nominal oscillation frequency of roughly 60 MHz based on process fabrication parameters. In addition to the capacitance sensor pixels, two reference sensors are also included on chip. These sensors have the same physical design but are placed within the outer padframe area of the chip, away from the active sensing area and physically isolated from the wet environment during experimentation.

An I^2C serial bus is implemented on chip and is used for data communication with an external readout system (microcontroller). This protocol requires two wires for data transfer and thus minimizes the number of connections required. This makes packaging and passivation of the bare chips simpler and more robust since there are fewer locations for possible passivation failure. Additionally, the I^2C protocol is designed to allow for multiple devices to share the same communication bus using the same number of wires, which can facilitate the future development of high throughput bioassays using several chips operating in parallel and sharing a communication bus. The entire array of sensor pixels is read out sequentially, and data collection continues unsupervised until a reset signal is triggered.

C. Sensor Resolution & Pixel Density

The output signals from each pixel are integrated using a counter for a fixed integration time in order to obtain the count value that is sent off chip. The minimum achievable sensor resolution (Δf_{min}) is inversely proportional to the integration time (T_i):

$$\Delta f_{\text{min}} = Q_{\text{min}}/T_i \tag{3}$$

where Q_{min} is the desired minimum difference in count value that corresponds to the minimum sensor resolution. Therefore, this design imposes a direct tradeoff between sensor speed and resolution. For typical operation the pixel sensitivity, based on simulations, is 1.22 MHz/fF [5]. Therefore, given a minimum target resolution and desired difference in count value, one can calculate the minimum required integration time. If the minimum target capacitance resolution is 10 aF ($\Delta f_{\text{min}} = 12.2$ kHz), and Q_{min} is set to 100, then the minimum integration time is 8.2 ms. However, in order to account for parasitics we have designed the system with a safety margin of two orders of magnitude, so the target T_i is 1 s. This integration time is set by a timing clock that is generated from frequency division of the system clock (f_{clk}). The system clock is generated off-chip by the readout microcontroller and is set to 3 MHz. The maximum integration clock frequency that satisfies these requirements is $f_{clk}/2^{22} = 0.72$ Hz, which means $T_i = 1.40$ s.

The pixels are sampled sequentially, so the overall sensor sampling rate is a function of the integration time and the number of pixels in the array. Therefore this design also imposes a direct tradeoff between the number of sensors in the array, the capacitance resolution, and the overall sensor speed. Biological cell dynamics occur on relatively slow timescales, so sampling intervals on the order of several minutes to an hour are appropriate [33], [34]. Using these guidelines, a maximum overall sampling interval of 1 minute is targeted. With this constraint the chip has been designed with an array of 16 sensors to allow for full chip readout within 30 seconds.

Increasing the number of sensors and thus pixel density will allow for greater spatial resolution and will facilitate averaging across sensors, at the cost of decreased temporal resolution. On the other hand, due to the relatively simple transduction mechanism of the chip, it is possible to increase the sampling rate using different methods such as simultaneous integration, parallel readout, and decreased integration time.

D. Fabricated Chip

Fig. 1(c) shows a photomicrograph of the system. The 4×4 array of pixels (shown in Fig. 1(d)) were arranged with an X and Y pitch of 196 μm and 186 μm, respectively, covering an area of 618×588 μm^2 on a 3×3 mm^2 chip. Since the electrodes are 30×30 μm^2 in size and are sensitive to permittivity changes in their immediate surroundings, the actual sensing area covered by the electrodes is roughly 120×120 μm^2. This means that the spatial resolution of the sensor is relatively low. However, when looking at the mechanics of the cell population as a whole, discrete measurement sites spread over a large area can suffice. Higher pixel density would be ideal for performing studies of individual cells. Eight I/O pads are used which were duplicated for packaging redundancy.

The readout system used in this work is a commercially available microcontroller (MicroPython PYB v1.0), although any device capable of I^2C communication can be used. All bias voltages are generated internally and the supply voltage of 3.3 V is provided by the microcontroller directly. The finite ramping time of the power supply and startup circuits built into the bias generator ensure the oscillators start up correctly. The microcontroller additionally supplies the digital clock signal that is used for timing of the controller logic on chip and the I^2C bus. Therefore no additional equipment besides the sensor, microcontroller, and a battery are required to perform measurements, allowing for experiments to be done easily outside of the laboratory setting. The average power consumption for the entire system was measured to be 300 mW with the IC chip consuming 8 mW. Therefore the complete lab-on-CMOS system can easily be implemented on a portable platform. In fact, a low power microcontroller can be used in order to extend battery lifetime to several days to facilitate longer term experiments.

IV. Benchtop Calibration

The proposed sensor was fabricated in a commercially available 0.35 μm CMOS process. Two bare dies were packaged in standard DIP-40 ceramic carriers and encapsulated in a low viscosity and high electrical resistivity epoxy (Cotronics Durapot 863). The passivation was done by first heating the chip-in-carrier to 120 °C and then manually applying the epoxy over the

bond wires and onto the chip surface, leaving only the sensing area uncovered. After curing, the epoxy creates a natural valley feature that aids in constraining cells to within the sensing area. Furthermore, by minimizing the number of required I/O pads, packaging is facilitated since there are fewer possible points of failure. Finally, wells to hold cell culture fluids were added to the devices. The wells were made from standard microbiology tubes (Eppendorf Flex Tube, 1.5 mL) that were cut and glued onto the package surface using a biocompatible silicone elastomer (Kwik-Cast Sealant, World Precision Instruments). The elastomer showed good adhesion (no fluid leakage was observed in any of the experiments conducted) and was chosen mainly due to its reversible bond which leaves no residue on the chips.

A. Sensor Calibration

The fabricated sensor transduces capacitive changes into a raw count value. In order to convert this output into a capacitance measurement, the count value was calibrated using a distance measurement platform [3]. A metal probe was placed over the sensor surface and its distance above the surface was controlled using a piezoelectric actuation platform. This mechanism had a distance resolution of 5 $\pm$ 0.5 μm. The experimental setup was simulated in a finite element method (FEM) solver (COMSOL Multiphysics) to estimate the capacitive loads induced at various probe positions. For the small operating range of interest (less than 2 fF) in cell sensing applications, the sensor output frequency response, *f(C)*, can be modeled linearly as follows:

$$f\left(C_{IN}\right) = -\alpha\left(C_{IN} + C_0\right) + f_0 \tag{4}$$

where C_{IN} is input capacitance, C_0 is the total of parasitic and offset capacitances at the circuit level, f_0 is a baseline frequency, and α is the sensor's sensitivity. The capacitive load measured due to the metal probe is then modeled using an inversely proportional relationship:

$$C_{IN}\left(x\right) = \beta/x + x' \tag{5}$$

where β is a scaling parameter that relates sensed capacitance to probe distance and *x'* is a parameter that accounts for passivation thickness and displacement errors introduced by the piezoelectric actuators. This leads to the following model of the output frequency as a function of probe distance:

$$f\left(x\right) = -\alpha\left(\frac{\beta}{x + x'} + C_0\right) + f_0 \tag{6}$$

Regressive fitting of this relationship was performed in order to generate a series of calibration curves that relate sensed capacitance to the measured output frequency. Fig. 2 shows such a curve that corresponds to the sensor's mean sensitivity with $\alpha = 590$ kHz/fF.

B. Sensed Capacitance Computation

Due to process variations and parasitics, each of the 16 sensor pixels are expected to have slightly different baseline frequency levels. Additionally, global changes such as supply levels and temperature cause drift in measured values. Therefore the final capacitance measurements are computed with respect to the reference pixel values, providing a pseudo-differential measurement. The data readout and signal processing performed on the results presented in this work are summarized as follows: 1) Subtract the baseline frequency for each pixel so that the initial value is set to a frequency of zero Hz; 2) subtract the reference from each sensor channel; 3) smooth the sensor response using a moving average filter (0.5% window span); 4) scale into units of capacitance using the calibrated sensitivity parameter, $\alpha = 590$ kHz/fF. The final sensed capacitance is described through:

$$\Delta C_N\left(t\right) = \alpha\, f_{sm}\left(x_N\left(0\right) - x_N\left(t\right) + x_{Ref}\left(0\right) - x_{Ref}\left(t\right)\right) \tag{7}$$

where $\Delta C_N(t)$ is the measured transient capacitance value for channel *N*, $x_N(t)$ is the raw data, and $x_{\text{Ref}}(t)$ is the reference channel. The smoothing operation, $f_{sm}(x(t))$, was performed to average over artificial readout artifacts in the data. These artifacts were caused by a design flaw in this chip, which had inadequate buffering in the digital readout chain that sometimes caused identical data to be repeated on the bus in two successive measurement cycles. When this occurred, it produced large spikes that were unrelated to the sensor readings. When this error occurs on the reference channel, it appears as correlated spikes when the capacitance is computed as in (7). These erroneous readings are relatively easy to identify and remove from the data stream. The window span of 0.5% samples in the smoothing filter corresponds to a roughly 15 minute data window over which averaging is performed. This value was chosen empirically to perform adequate smoothing based on the overall sampling rate while being small enough to not obscure changes due to cells. It is important to note again that the relationship in (7) is valid only for small ($<$2 fF) changes in capacitance.

As a test of sensor stability, cell culture media was put into the sample well and the device was placed in an incubator at 37 °C for 15 hours. The pixels oscillate with baseline frequencies ranging between 57.99–60.50 MHz. When the offsets between these baseline frequencies are accounted for, the maximum frequency drift over 15 hours for a single pixel is 32.7 kHz. The mean frequency drift over all pixels is 4.7 kHz. The mean standard deviation of frequency over all pixels was calculated to be 8.56 kHz, which corresponds to a dynamic capacitance variation of 14.4 aF.

The temperature dependence of the sensor was analyzed as well. A device with cell culture media was placed into an oven. Data was recorded as the device heated up to 45 °C. The mean frequency across pixels is shown in Fig. 3. The change is approximately linear over this temperature range. A linear fit of the data shows a temperature dependence of -129 kHz/°C, which translates to a shift of -217 aF for a 1 °C change in temperature. However, when the reference pixels are used to account for the temperature drift, the temperature dependence reduces to 19 kHz/°C, which corresponds to 32 aF/°C. This value limits the attainable sensor resolution. In real experiments, the device will usually be placed in a temperature-controlled environment which will minimize temperature dependency. Furthermore the thermal mass of the cell culture media limits local temperature fluctuations.

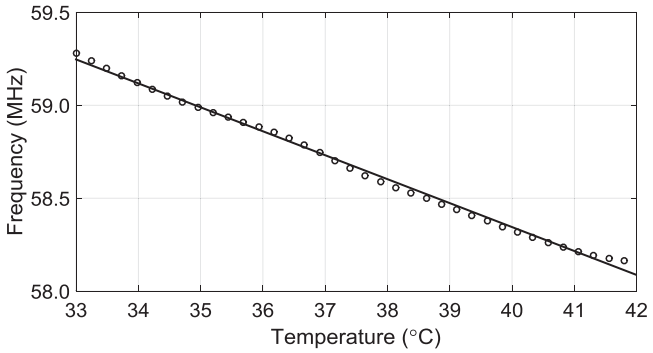

Fig. 3. Temperature dependence of sensor. Points show mean response over pixels and solid line shows linear fit. The sensor shows a sensitivity of 129 kHz/°C.

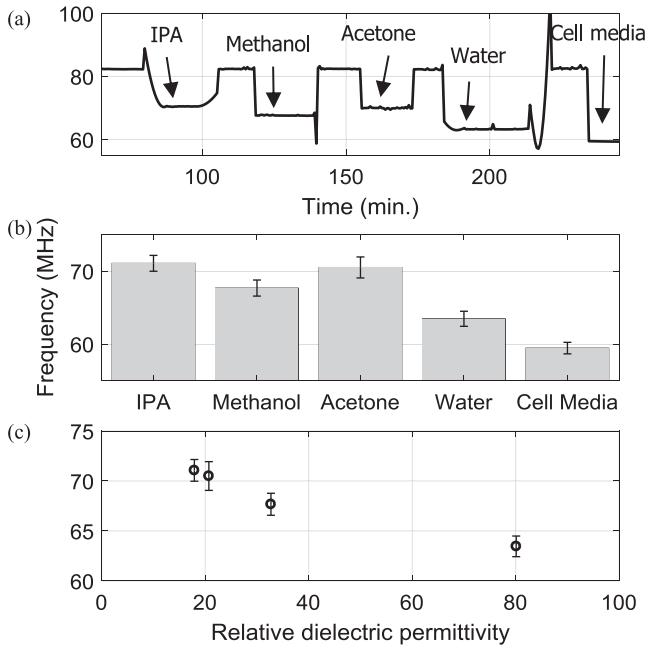

Fig. 4. Sensor response to addition of different fluids. (a) Transient plot of response for a single pixel. (b) Mean response and standard deviation across 16 pixels. (c) Mean response as a function of relative dielectric permittivity.

C. Response to Organic Solvents

The packaged chip was evaluated by measuring the response to fluids placed in the sample well. We selected fluids with a range of dielectric constants in order to induce changes in permittivity of the environment surrounding the chip, causing changes in signal output. The fluids were deionized (DI) water ($\varepsilon_r = 80.1$), acetone ($\varepsilon_r = 20.7$), methanol ($\varepsilon_r = 32.7$), and isopropyl alcohol (IPA) ($\varepsilon_r = 17.9$) [35]. Cell media was also used. Fig. 4(a) shows data from a representative pixel that illustrates the application and removal of each fluid over time. Fluids with higher relative permittivity induce a stronger drop in amplitude from the baseline (air, $\varepsilon_r = 1.0$) since they correspond to a larger sensed capacitance. Of the tested solutions, DI water has the highest relative permittivity and causes a change in capacitance of 12 fF from the baseline, based on FEM simulations. Therefore the input range of the sensor as tested in this work is 12 fF. The sharp features seen in Fig. 4(a) are artifacts related to physical movements in the experiment. This is especially the case with acetone since its relatively high vapor pressure means constant fluid replenishment is needed if the package is not sealed. Fig. 4(b) shows the mean sensor output across all 16 pixels with error bars marking standard deviations, and Fig. 4(c) shows the response as a function of relative dielectric permittivity.

V. *In Vitro* Measurements

A. Experimental Protocol

Preliminary biological tests were performed by growing adherent cells onto the chip array. Growth media (RPMI 1640) was prepared with 10% fetal bovine serum and supplemented with antibiotics and anti-fungals (penicillin and streptomycin). Two human ovarian cancer cell lines were used in this experiment, CP70 and A2780. The cells were grown in a cell culture vessel until they reached log phase growth. At this point the cells were detached using 0.25% trypsin/EDTA, formed into a pellet and re-suspended into 12 mL of fresh cell media. The devices were prepared by sterilizing them with UV light, then rinsing them with deionized water, phosphate buffer solution (Dulbecco's Phosphate Buffer Solution), and cell media. Fresh media was then added and the device was maintained in an incubator (37 °C, 5% CO_2) for 15 minutes. Then 40 μL of the cell suspension was added to the device, and data was continuously recorded throughout the experiment. Fig. 5(b) shows a photomicrograph of CP70 cells cultured on the sensor, after 21 hours of growth. Two separate devices were packaged and plated with each of the two cell lines in separate experiments, resulting in a total of four experimental datasets. All 16 sensor pixels on each chip were active and recording. The devices were kept in the incubator and connected to the readout microcontroller and laptop (located externally) using a shielded Ethernet cable.

B. Tracking Cell Adhesion

Fig. 5(a) shows response curves obtained from a device plated with CP70 cells. Each trace corresponds to an individual pixel labeled by its (row, column) address. The two vertical lines at $t = 21$ hours and $t = 44$ hours indicate time points when recording was paused to take images of the chip's surface, shown in Fig. 5(b) and (c). (High resolution images are provided as supplementary material in Figs. S1 and S2). For all but one sensor, the signal remained relatively low until 5 hours of incubation. This is consistent with the pre-adhesion phase of growth, during which cells settle onto the chip surface. After this phase, cells start adhering to the chip surface, showing a corresponding increase in signal. The strength of the signal change is indicative of the quality of cell growth at that pixel, which in turn depends on where the cells first settle down from the solution. Therefore certain pixels show little change in signal if no initial settling (and subsequent adhesion) occurs. This is evident in sensor (2,1) which shows little change through 34 hours of incubation. Fig. 5(b) shows the corresponding absence of nearby cells at

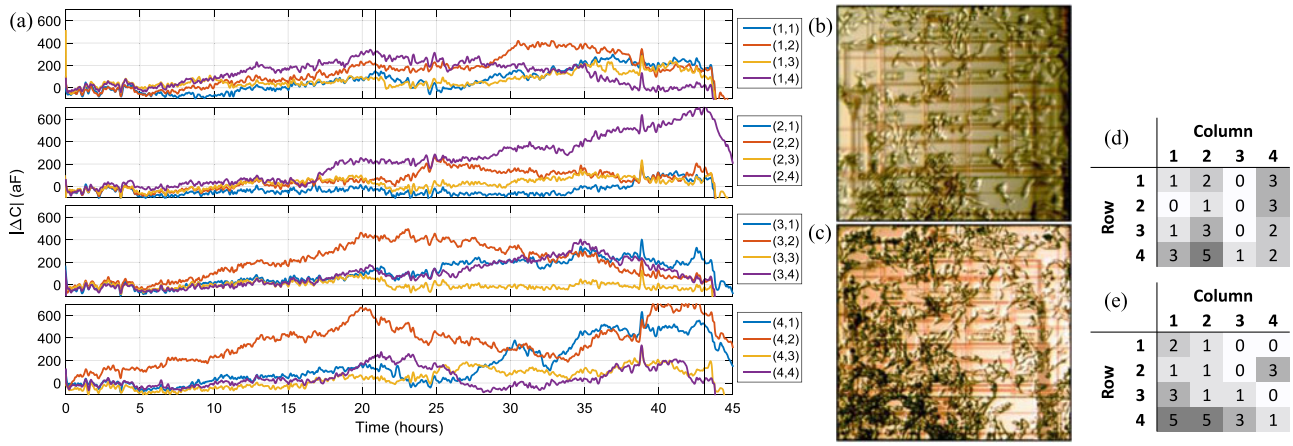

Fig. 5. (a) Response curves of Device 1 as CP70 cells adhere and proliferate across the sensor array in (row, column) notation. The two vertical black lines at $t = 21$ hours and $t = 44$ hours indicate times when data recording was paused for imaging. Middle panel shows the corresponding images after (b) 21 hours, and (c) 44 hours of incubation of CP70 cells. Images were used to quantify cell coverage which are shown in (d) and (e).

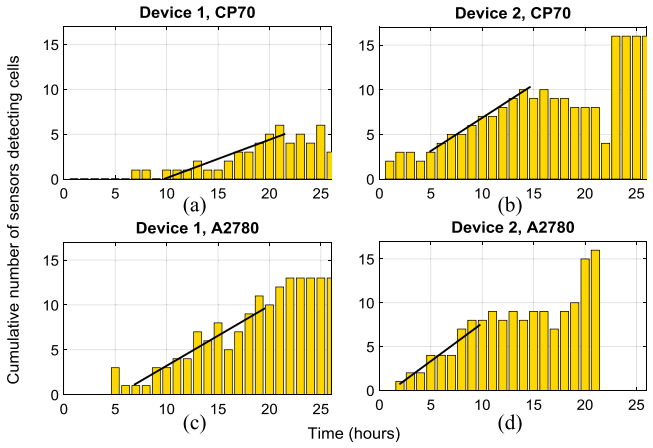

Fig. 6. Cumulative number of sensors that show an increase in capacitance as a function of time, for each of the four experiments described in Section V-A. The large plateau after 22 hours in (b) is due to solution evaporation.

this pixel. Likewise, the response of sensor (3, 3) stays below 50 aF through 44 hours of incubation. Both Fig. 5(b) and (c) show this pixel to have no cells directly on top of the sensing electrodes.

A second experiment was conducted using A2780 cells (Sensor response data is provided as supplementary material in Fig. S3). Two pixels were identified as having no cell coverage over their electrodes from images of the chip surface. The mean response of these empty pixels is compared to that of all other sensors and shows a peak signal difference of 480 aF. When the empty pixels are compared to pixels with nearly complete coverage of their electrodes, the difference increases to 640 aF. This supports positive correlation of sensor response with cell coverage.

The growth rate of cells can be monitored by looking at the cumulative number of sensors (N_{CS}) in the array that record a significant change in capacitance, designated by a threshold value, during the experiment. Fig. 6 shows such a plot with the

TABLE I
CELL GROWTH RATE ESTIMATION

Cell Line	*Device*	*Adhesion Time (hrs)*	*Growth Rate (sensors/hr)*	*Growth Rate (μm^2 /hr)*
CP70	1	11.7	0.43	380
CP70	2	9.8	0.74	670
A2780	1	12.7	0.67	600
A2780	2	7.8	0.87	780

capacitance threshold set at 200 aF (>10 times the noise threshold of 8.56 kHz, Section IV–B), for each of the four experiments. For clarity, the increments were recorded for each hour of incubation. As can be seen, there is an initial 5 hour period where a small number (<5) of sensors show a capacitance change. This is indicative of the cell sedimentation process. Then as the cells adhere and proliferate, the number of sensors showing a response greater than 200 aF increases. Over the course of several hours the number of affected sensors increases and plateaus.

A quantitative estimate of the cell growth rate can be obtained by calculating the rate at which sensors detect cells over the course of the adhesion. The slope of N_{CS} for each of the experiments in Fig. 6 was calculated; the solid lines show the calculated slope line. A nominal area growth rate can then be estimated by scaling this growth rate by the known $30 \times 30\ \mu m^2$ area of each pair of electrodes. Table I summarizes the estimated growth rate for each of the experiments.

C. Cell Migration

As cells adhere and proliferate, they can also move from one location to another, a phenomenon called cell migration [36]. This can also be observed in the transient response curves of Fig. 5(a). As cells proliferate and cover more electrode area, a corresponding increase in absolute sensed capacitance is observed. Likewise if cells migrate away from an electrode, they

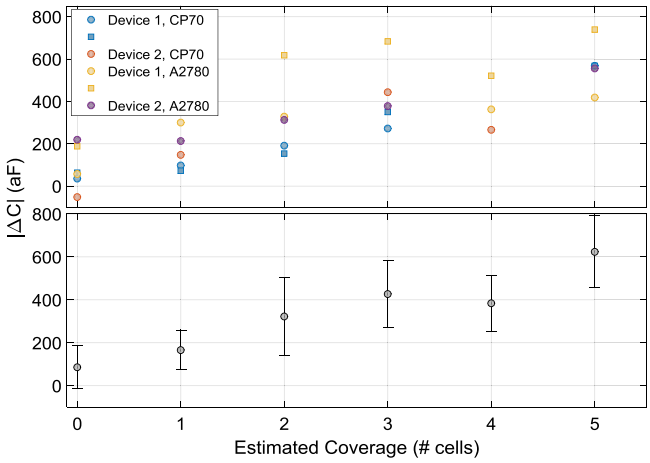

Fig. 7. Plot of the measured sensor response as a function of estimated cell coverage of pixels. (a) All experiments separately, (b) Mean value. Linear fit shows a sensitivity of 100 aF/cell.

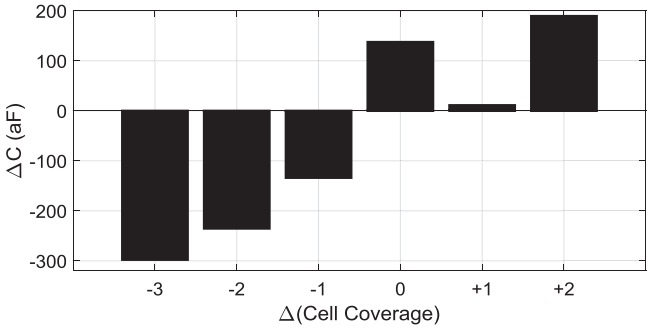

Fig. 8. Plot of the measured change in capacitance as a function of change in cell coverage (Device 1, CP70 cells).

cover less electrode area, causing a corresponding decrease in signal. Several sensor channels show signal fluctuations over a period of several hours. These changes can be caused by cell migration to and away from the electrodes. For example, sensor $(1, 4)$ shows a gradual signal drop from 300 aF to 20 aF between $t = 21$ hours and $t = 44$ hours. Examination of the images in Fig. 5(b) and (c) shows a corresponding decrease in the number of cells on sensor $(1, 4)$ between these two time-points. Sensors $(3, 2)$ and $(4, 4)$ also exhibit this behavior, with decreases of 392 aF and 226 aF, respectively.

D. Quantifying Cell Coverage

In order to validate the signals obtained from the sensor, cell coverage was estimated by analyzing images of the chip during the recording sessions. These images were taken using a standard reflective microscope with a long (>55 mm) working distance objective. The number of cells covering each pixel was estimated and recorded. A more precise count of cells would require higher resolution microscopy. Fig. 7(a) shows the measured sensor outputs as a function of the estimated cell coverage. In two of the experiments, a second image of the chip array was taken 24 hours after the first image, providing a second time point for cell coverage quantification.

The experimental data shows a clear pattern of cell coverage detection; as a larger area of a pixel's electrodes are covered, a corresponding increase in the sensor signal is recorded. Fig. 7(b) shows the average capacitance change across all experiments. A linear fit ($R^2 = 0.94$) estimates a response of 100 aF/cell. Error bars corresponding to the standard deviation of the measurements indicate that variability is relatively large compared to the mean: ± 200 aF for 2 cell coverage. However, since the experiments vary in both device used and type of cells cultured, discrepancies are expected. The dynamic change in measured capacitance also has strong correlation with changes in cell coverage. Fig. 8 shows such a plot for the experiment with Device 1 and CP70 cell line. The change in measured capacitance (ΔC) is the difference in signal between two time points that correspond to the two images. The change in cell coverage is the difference in the estimated number of cells covering each pixel at the two time points. For this experiment the change in coverage ranged from -3 to $+2$ cells.

As can be seen there is a correlation between the change in cell coverage and the change in measured capacitance. An average decrease of 300 aF in the signal was observed for sensors that showed a 3 cell decrease in coverage between the two time points, and a 130 aF decrease for sensors exhibiting a single cell decrease in coverage. However an average signal increase of 140 aF was measured for sensors that had no change in coverage. We note that the cell coverage estimates were obtained manually and reflect an estimate of the number of cells on the electrode, so reported changes in cell coverage are limited in accuracy. In future work, higher resolution imagery and image processing may be used to improve estimates of coverage and to extend estimates to incremental changes in cell coverage due to proliferation and migration.

VI. Discussion

The design and characterization of a lab-on-CMOS system-on-chip has been presented along with validation from live cell experiments. While this is an important step forward, we highlight some open questions about the characterization of biological results.

A. Validation

In order to obtain accurate cell coverage information, it is important to be able obtain visual confirmation of what is occurring on the sensor surface. This is especially important since capacitive changes are the result of changes in the permittivity of the immediate surroundings of the input electrodes, which could result from the adhesion of cells or changes in the liquid media. This work relied on manual observation of cells based on photomicrographic images. There are a few problems with this approach. Visual identification is inherently subjective since it is difficult to make estimates that are consistent across multiple electrodes and throughout multiple trials. Therefore in future work it is important to develop techniques for objective quantification of the cell coverage, both number of cells and their

surface area. In this work the images were obtained under white light illumination using a Nikon Zoom Stereomicroscope with magnification of 8X and a ring light. Fluorescence microscopy might be used to better highlight viable cells, although this would be done as an end-point assay.

A major obstacle to validation based on visual observation is the difficulty in obtaining clear images of the sensor surface. Since the sensor substrate is opaque, imaging techniques that require a through-sample optical path cannot be used. These include the techniques of phase contrast and inverted light microscopy that are normally used in microbiology. This means that reflective microscopy is required. However, acquiring clear images with this method is difficult due to light refraction through the air-liquid interfaces, as can be seen in Fig. 5(b) and (c). In order to mitigate this problem, higher-quality images may be obtained using a microscope with immersion lenses and differential interference contrast analysis [1].

Another important consideration in validating the biosensor is having higher temporal resolution of the images. This implies continual imaging of the sensor surface during the entire course of the experiments. This introduces logistical difficulties since the sensor would need to be moved to an imaging station numerous times during a recording session. The physical movement inevitably introduces mechanical disturbances, which could compromise the viability of cells. An alternative imaging paradigm would implement real-time imaging within the incubator. Several research and commercial grade systems exist that integrate cell culture incubator conditions and imaging [37]–[41]. However, these systems have been implemented using inverted microscopes and therefore cannot be used in performing live-cell experiments with the lab-on-CMOS system. In future work, we plan to explore experimental enhancements to imaging from fluorescence microscopy, immersion lenses, and continual imaging.

B. Sources of Variability

Capacitance measurements have numerous sources of variability. First, the sensed capacitance is a function of the dielectric properties of the environment surrounding the input electrodes. This means the device is sensitive to all of the materials above the chip's passivation layer, including media solution, non-biological particles in the media, and the cells themselves. Evaporation of cell media from the top of the sensor will thus affect sensor response. For example in Fig. 6(b), the plateau after 22 hours is due to a large baseline shift in sensor response as the solution evaporated. There are several ways to mitigate evaporation in the sample well. These include maintaining high humidity levels in the environment to reduce the evaporation rate, adding pre-warmed media to the sample well during the course of the experiments, and covering the well surface with mineral oil. One method used in subsequent experiments has been to place a semi-permeable membrane (Nunc EasYFlask Filter Cap) on top of the well. These membranes prevent evaporation of media while allowing for gas exchange. These membranes have been used with success in preventing evaporation in tests with only media solution lasting over one week.

TABLE II
STATE OF THE ART COMPARISON TABLE

Ref.	[21]	[30]	[27]	[24]	This work
Method	CS	CBCM	CS	CF	CF
Tech. (μm)	0.5	0.35	0.25	0.25	0.35
Organism	Bovine aortic smooth muscle	Human lung carcinoma, H1299	Bacteria, *Staphylococcus epidermidis*	Bacteria, *Staphylococcus epidermidis*	Human ovarian cancer, CP70/A2780
Sensitivity	-	320 mV/fF	55 mV/fF	-	590 kHz/fF
Resolution	-	10 aF	450 aF	5 fF	14.4 aF
Cell Response (max.)	23 fF	6.3 fF*	700 aF* 62 aF/cell	-	620 aF; 100 aF/cell

*estimate based on reported sensitivity and presented measurement results

Additionally, for the frequency-based sensor presented in this work, temperature, power supply, parasitics, and threshold voltage variations can all introduce uncertainty into the measurements [42], [43]. These parameters can shift the baseline frequency response of the oscillators to cells/media, and contribute to each pixel's dynamic responses to capacitive changes. Sensitivity to temperature can be mitigated by careful control of the overall chip package's temperature using the temperature-controlled incubator. Power supply fluctuations can be mitigated by using high performance low dropout voltage regulators to supply the power rails with decoupling capacitors to minimize ripple. The effects of fabrication process variations mean that per-pixel calibration needs to be performed for this sensor. As described above, variability to these factors has been significantly reduced using pseudo-differential measurements with respect to reference sensors placed outside the active sensing area of the chip.

VII. SUMMARY AND CONCLUSION

In this work a CMOS capacitance sensor chip was designed for the measurement of capacitive changes of cells. The sensor circuitry and system level architecture were discussed. Two separate devices were packaged for live cell experiments. *In vitro* tests were then performed on the devices using human ovarian cancer cell lines CP70 and A2780. Microscopic images were taken of the sensor surfaces during the experiments to provide visualization of cell growth and proliferation.

Analysis of the data showed transient capacitive changes during experiments which correlated with visual images of the chip. Estimates of the cell growth rate were obtained from analysis of the transient data for each experiment. Cell migration was also observed at some sensor locations. Finally, the sensitivity of the sensors was quantified by comparing the measured capacitance responses to the cell coverage at each individual pixel. Analysis of four experiments showed good correlation between cell coverage and change in capacitance measurement. Table II shows a comparison between state-of-the-art studies that performed *in vitro* experiments and the sensor studied in this work.

This study has demonstrated the continued promise of monitoring cell viability using a cell capacitance transduction mechanism. The use of a lab-on-CMOS technology allows for a flexible and compact measurement tool that can be used in a variety of applications, such as drug efficacy monitoring, biofilm growth, and medical diagnosis.

ACKNOWLEDGMENT

The authors would like to thank Dr. Y. Shu from The University of Maryland, School of Pharmacy for graciously providing the human ovarian cancer cells used in this study, and the Center of Microscopy and Nanotechnology, University of Oulu for technical support.

REFERENCES

[1] T. Datta-Chaudhuri, E. Smela, and P. A. Abshire, "System-on-chip considerations for heterogeneous integration of CMOS and fluidic bio-interfaces," *IEEE Trans. Biomed. Circuits Syst.*, vol. 10, no. 6, pp. 1129–1142, Dec. 2016.

[2] Y. H. Ghallab and Y. Ismail, "CMOS based lab-on-a-chip: Applications, challenges and future trends," *IEEE Circuits Syst. Mag.*, vol. 14, no. 2, pp. 27–47, Apr.–Jun. 2014.

[3] B. Senevirathna, S. Lu, and P. Abshire, "Characterization of a high dynamic range Lab-on-CMOS capacitance sensor array," in *Proc. IEEE Int. Symp. Circuits Syst.*, 2017, pp. 1–4.

[4] E. Naviasky, T. Datta-Chaudhuri, and P. Abshire, "High resolution capacitance sensor array for real-time monitoring of cell viability," in *Proc. IEEE Int. Symp. Circuits Syst.*, 2014, pp. 634–637.

[5] B. Senevirathna, A. Castro, M. Dandin, E. Smela, and P. Abshire, "Lab-on-CMOS capacitance sensor array for real-time cell viability measurements with i2c readout," in *Proc. IEEE Int. Symp. Circuits Syst.*, 2016, pp. 2863–2866.

[6] C. K. Miranti and J. S. Brugge, "Sensing the environment: a historical perspective on integrin signal transduction," *Nature Cell Biol.*, vol. 4, no. 4, pp. E83–E90, 2002.

[7] C. O'Connor, J. U. Adams, and J. Fairman, *Essentials of Cell Biology*. Cambridge, MA, USA: NPG Edu., 2014.

[8] J. P. Johnson, "Cell adhesion molecules in the development and progression of malignant melanoma," *Cancer Metastasis Rev.*, vol. 18, no. 3, pp. 345–357, Sep. 1999.

[9] G. Gabbiani, "The myofibroblast in wound healing and fibrocontractive diseases," *J. Pathology*, vol. 200, no. 4, pp. 500–503, 2003.

[10] U. Cavallaro and G. Christofori, "Cell adhesion and signalling by cadherins and Ig-CAMs in cancer," *Nature Rev. Cancer*, vol. 4, no. 2, pp. 118–132, 2004.

[11] M. Dembo and Y.-L. Wang, "Stresses at the cell-to-substrate interface during locomotion of fibroblasts," *Biophys. J.*, vol. 76, no. 4, pp. 2307–2316, 1999.

[12] E. W. K. Young, A. R. Wheeler, and C. A. Simmons, "Matrix-dependent adhesion of vascular and valvular endothelial cells in microfluidic channels," *Lab Chip*, vol. 7, no. 12, pp. 1759–1766, 2007.

[13] K. V Christ, K. B. Williamson, K. S. Masters, and K. T. Turner, "Measurement of single-cell adhesion strength using a microfluidic assay," *Biomed. Microdevices*, vol. 12, no. 3, pp. 443–455, Jun. 2010.

[14] R. A. Hoebe, C. H. Van Oven, T. W. J. Gadella, P. B. Dhonukshe, C. J. F. Van Noorden, and E. M. M. Manders, "Controlled light-exposure microscopy reduces photobleaching and phototoxicity in fluorescence live-cell imaging," *Nature Biotechnol.*, vol. 25, no. 2, pp. 249–253, Feb. 2007.

[15] L. Balasubramanian, K.-P. Yip, T.-H. Hsu, and C.-M. Lo, "Impedance analysis of renal vascular smooth muscle cells.," *Amer. J. Physiol. Cell Physiol.*, vol. 295, pp. C954–C965, 2008.

[16] J. Wegener, A. Janshoff, and H. J. Galla, "Cell adhesion monitoring using a quartz crystal microbalance: Comparative analysis of different mammalian cell lines," *Eur. Biophys. J.*, vol. 28, no. 1, pp. 26–37, 1999.

[17] M. Saitakis and E. Gizeli, "Acoustic sensors as a biophysical tool for probing cell attachment and cell/surface interactions," *Cellular Mol. Life Sci.*, vol. 69, no. 3, pp. 357–371, 2012.

[18] M. L. Pourciel-Gouzy, W. Sant, I. Humenyuk, L. Malaquin, X. Dollat, and P. Temple-Boyer, "Development of pH-ISFET sensors for the detection of bacterial activity," *Sensors Actuators B Chem.*, vol. 103, no. 1–2, pp. 247–251, 2004.

[19] K. Niitsu, S. Ota, K. Gamo, H. Kondo, M. Hori, and K. Nakazato, "Development of microelectrode arrays using electroless plating for CMOS-based direct counting of bacterial and HeLa cells," *IEEE Trans. Biomed. Circuits Syst.*, vol. 9, no. 5, pp. 607–619, Oct. 2015.

[20] S. B. Prakash and P. Abshire, "A CMOS capacitance sensor that monitors cell viability," in *Proc. IEEE Sensors*, 2005, vol. 2005, pp. 1177–1180.

[21] S. B. Prakash and P. Abshire, "On-chip capacitance sensing for cell monitoring applications," *IEEE Sens. J.*, vol. 7, no. 3, pp. 440–447, Mar. 2007.

[22] E. Ghafar-Zadeh and M. Sawan, "Charge-based capacitive sensor array for CMOS-based laboratory-on-chip applications," *IEEE Sens. J.*, vol. 8, no. 3–4, pp. 325–332, Apr. 2008.

[23] L. Yang and R. Bashir, "Electrical/electrochemical impedance for rapid detection of foodborne pathogenic bacteria," *Biotechnol. Adv.*, vol. 26, no. 2, pp. 135–150, 2008.

[24] N. Couniot, D. Bol, O. Poncelet, L. A. Francis, and D. Flandre, "A capacitance-to-frequency converter with on-chip passivated microelectrodes for bacteria detection in saline buffers up to 575 MHz," *IEEE Trans. Circuits Syst. II, Express Briefs*, vol. 62, no. 2, pp. 159–163, Feb. 2015.

[25] E. Ghafar-Zadeh, M. Sawan, V. P. Chodavarapu, and T. Hosseini-Nia, "Bacteria growth monitoring through a differential CMOS capacitive sensor," *IEEE Trans. Biomed. Circuits Syst.*, vol. 4, no. 4, pp. 232–238, Aug. 2010.

[26] G. Nabovati, E. Ghafar-Zadeh, and M. Sawan, "A novel multifunctional integrated biosensor array for simultaneous monitoring of cell growth and acidification rate," in *Proc. IEEE Int. Symp. Circuits Syst.*, 2016, pp. 2855–2858.

[27] N. Couniot, L. A. Francis, and D. Flandre, "A 16x16 CMOS capacitive biosensor array towards detection of single bacterial cell," *IEEE Trans. Biomed. Circuits Syst.*, vol. 10, no. 2, pp. 364–374, Apr. 2016.

[28] S. B. Prakash and P. Abshire, "A fully differential rail-to-rail capacitance measurement circuit for integrated cell sensing," in *Proc. IEEE Sensors*, 2007, pp. 1444–1447.

[29] G. Nabovati, E. Ghafar-Zadeh, M. Mirzaei, G. Ayala-Charca, F. Awwad, and M. Sawan, "A new fully differential CMOS capacitance to digital converter for lab-on-chip applications," *IEEE Trans. Biomed. Circuits Syst.*, vol. 9, no. 3, pp. 353–361, Jun. 2015.

[30] G. Nabovati, E. Ghafar-zadeh, A. Letourneau, and M. Sawan, "Towards high throughput cell growth screening: A new CMOS 8×8 biosensor array for life science applications," *IEEE Trans. Biomed. Circuits Syst.*, vol. 11, no. 2, pp. 380–391, Apr. 2017.

[31] S. B. Prakash and P. Abshire, "A fully differential rail-to-rail CMOS capacitance sensor with floating-gate trimming for mismatch compensation," *IEEE Trans. Circuits Syst. I, Reg. Papers*, vol. 56, no. 5, pp. 975–986, May 2009.

[32] B. Andreev, E. L. Titlebaum, and E. G. Friedman, "Sizing CMOS inverters with miller effect and threshold voltage variations," *J. Circuits, Syst. Comput.*, vol. 15, no. 3, pp. 437–454, 2006.

[33] P. Jain, R. A. Worthylake, and S. K. Alahari, "Quantitative analysis of random migration of cells using time-lapse video microscopy," *J. Vis. Exp.*, no. 63, pp. 1–11, 2012.

[34] N. Wick, S. Thurner, K. Paiha, R. Sedivy, I. Vietor, and L. A. Huber, "Quantitative measurement of cell migration using time-lapse videomicroscopy and non-linear system analysis," *Histochem. Cell Biol.*, vol. 119, no. 1, pp. 15–20, Jan. 2003.

[35] Univ. Washington, "Dielectric constants of common solvents," Dielectrical Constants Solvents, 2017.

[36] R. J. Petrie, A. D. Doyle, and K. M. Yamada, "Random versus directionally persistent cell migration," *Nature Rev. Mol. Cell Biol.*, vol. 10, no. 8, pp. 538–549, 2009.

[37] D. Jin *et al.*, "Compact wireless microscope for in-situ time course study of large scale cell dynamics within an incubator," *Sci. Rep.*, vol. 5, no. 1, 2016, Art. no. 18483.

[38] Nikon Instrum., Inc, "Nikon biostation IM-Q," 2017.

[39] World Precis. Instrum., "Microscope environmental chamber, heat and CO2 controller," 2017.

[40] GE Healthcare Life Sci., "Cytell cell imaging system," 2017.

[41] Leica Microsyst., "Inverted microscope platform leica DMi8," 2017.

[42] M. Mandal and B. Sarkar, "Ring oscillators: Characteristics and applications," *Indian J. Pure Appl. Phys.*, vol. 48, no. Feb., pp. 136–145, 2010.

[43] A. A. Abidi, "Phase noise and jitter in CMOS ring oscillators," *IEEE J. Solid-State Circuits*, vol. 41, no. 8, pp. 1803–1816, Aug. 2006.

Bathiya Prashan Senevirathna (S'08) received the B.S. degree in electrical engineering from Howard University, Washington, DC, USA, in 2012. He is currently working the Ph.D. degree in electrical engineering at the University of Maryland, College Park, MD, USA, where he is a Graduate Research Assistant in the Integrated Biomorphic Information Systems Laboratory. He has previously had internships at the Princeton Plasma Physics Laboratory, Princeton, NJ, USA, and the National Institutes of Health, Bethesda, MD, USA. His research interests include mixed-signal integrated circuit design, CMOS biosensors, and their integration toward lab-on-chip technology.

Mr. Senevirathna was the Vice-President for the IEEE student society with Montgomery College, Rockville, MD, USA, and Howard University. He is a Member of the IEEE-HKN and Tau Beta Pi.

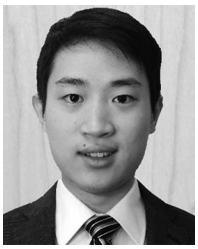

Sheung Lu (S'13) was born in Maryland, USA, in 1994. He received the B.S. degree in computer engineering from the University of Maryland, Baltimore, MD, USA, in 2016. He is currently working toward the Ph.D. degree in electrical engineering at the University of Maryland, College Park, MD, USA, where his research focuses on CMOS biosensors for cell viability measurements. His research interests include computational sensing, mixed-signal very large scale integration systems, and lab-on-CMOS applications.

Marc P. Dandin (S'09–M'13–SM'17) received the B.S. and M.S. degrees in electrical engineering, and the Ph.D. degree in bioengineering, both from the University of Maryland, College Park, MD, USA. His Ph.D. dissertation focused on the development of single-photon avalanche diodes in standard CMOS technologies and on the integration of these sensors in bioanalytical microsystems. He has more than 15 years of research experience in electrical engineering, mechanical engineering, and bioengineering. Further, he has more than 5 years of experience in patent preparation and prosecution of semiconductor-related inventions on behalf of several fortune 500 companies. He has contributed to more than 30 archival publications and has presented at numerous international workshops and conferences on semiconductors and circuits. He is a Technology Entrepreneur and the founder and CEO of Kiskeya Microsystems, Rockville, MD, USA. He is an inventor of several patents and patent applications assigned to Kiskeya Microsystems. He is an Adjunct Professor in electrical engineering with The George Washington University, Washington, DC, USA, where he teaches an advanced graduate course in analog VLSI electronics.

Dr. Dandin was on the Industrial Board of the 2017 IEEE International Symposium on Circuits and Systems Conference. He is currently the Secretary of the IEEE Circuits and Systems chapter of the Washington, DC, Northern Virginia, and Maryland regions. Furthermore, he was a Technical Reviewer for several IEEE journals, including the IEEE SENSORS JOURNAL and the IEEE ELECTRON DEVICE LETTERS. He was the recipient of the 2008 Fischell Fellowship in Biomedical Engineering and the 2011 inaugural Jimmy H. C. Lin Award for Entrepreneurship.

John Basile was born in Brooklyn, NY, USA, on June 5, 1967. He received the B.A. degree in biology from Cornell University, Ithaca, NY, USA, in 1989, the D.D.S. degree from the State University of New York at Stony Brook, School of Dental Medicine, Stony Brook, NY, USA, in 1993, and the D.M.Sc. degree with a concentration in pathology at Harvard University School of Dental Medicine, Boston, MA, USA, in 2002.

From 2002 to 2007, he was a Postdoctoral Research Fellow with the Oral and Pharyngeal Cancer Branch, National Institute of Craniofacial Research, National Institutes of Health, Bethesda, MD, USA. He is currently an Associate Professor with the Department of Oncology and Diagnostic Sciences, University of Maryland School of Dental Medicine, Baltimore, MD, USA. He is the author of several publications and book chapters on pathological angiogenesis, local tumor invasion, and skeletal metastasis.

Dr. Basile is a Member of the Molecular and Structural Biology group of the Marlene and Stuart Greenebaum Cancer Center, University of Maryland School of Medicine, Baltimore, MD, USA, the American Association of Cancer Research, and the American Association of Oral and Maxillofacial Pathology. He has been boarded by the American Board of Oral and Maxillofacial Pathology since 2008.

Elisabeth Smela (M'87) received the B.S. degree in physics from Massachusetts Institute of Technology, Cambridge, MA, USA, and the Ph.D. degree in electrical engineering from the University of Pennsylvania, Philadelphia, PA, USA. She then worked at Linköping University in Sweden, Risø National Lab in Denmark, and Santa Fe Science and Technology, Santa Fe, NM, USA, before joining the Department of Mechanical Engineering, The University of Maryland, College Park, MD, USA. Her research utilizes organic materials in devices and include microfabricated conjugated polymer artificial muscles, dielectrophoresis, electro-osmotic actuators, cell-based sensing, and elastomeric sensors.

Pamela A. Abshire (S'98–M'02–SM'16–F'18) received the B.S. degree (with honors) in physics from California Institute of Technology, Pasadena, CA, USA, in 1992, and the M.S. and Ph.D. degrees in electrical and computer engineering from The Johns Hopkins University, Baltimore, MD, USA, in 1997 and 2002, respectively.

From 1992 to 1995, she was with the Bradycardia Research Department, Medtronic, Inc. Since 2001, she has been with the Department of Electrical and Computer Engineering and the Institute for Systems Research, The University of Maryland, College Park, MD, USA, where she is currently a Professor. Her research focuses on low-power mixed-signal integrated circuit design, adaptive integrated circuits, integrated circuits for biosensing, hybrid devices incorporating chips and biological components, and understanding the tradeoffs between performance and energy in natural and engineered systems.

Dr. Abshire is on the Emerging Technologies and Research Advisory Committee for the U.S. Department of Commerce and on the Board of Governors of the IEEE Circuits and Systems Society.